High-pressure evolution of the magnetic order in $LaMnO_3$

D. P. Kozlenko,[1,*] E. V. Lukin,[1] S. E. Kichanov,[1] Z. Jirák,[2] N. O. Golosova,[1] and B. N. Savenko[1]
[1]*Frank Laboratory of Neutron Physics, JINR, 141980 Dubna, Russia*
[2]*Institute of Physics, Academy of Sciences, 16253 Prague, Czech Republic*

(Received 27 September 2022; revised 3 April 2023; accepted 6 April 2023; published 21 April 2023)

A relationship between evolution of the long-range magnetic order, crystal structure, and lattice distortions in $LaMnO_3$ was studied by a combination of neutron diffraction and Raman spectroscopy at high pressures up to 39 and 50 GPa, respectively, covering the temperature range 5 to 290 K. The Raman spectra reveal a gradual structural phase transformation evolving in the pressure range of 4 to 17 GPa, caused by a modification of the Jahn-Teller (JT) lattice distortions from the static cooperative character to the local one. A presence of residual JT-distorted regions associated with the initial phase is detected up to 32 GPa, where the insulator-metal transition occurs. At higher pressure, the local JT distortions also vanish completely at further compression up to 50 GPa. In the neutron diffraction data, a strong suppression of the A-type antiferromagnetic (AFM) phase is observed over the pressure region of the phase transformation. This is accompanied by a noticeable reduction in magnitude of the Q_2 and Q_3 JT local modes. The effective ordered magnetic manganese moment is reduced about twice at pressures up to 14 GPa. At higher pressures up to 30 GPa, residual regions of the A-type AFM phase coexist with the magnetically disordered phase. In the range 30 to 39 GPa, i.e., during the pressure-induced insulator-metal transition, these regions disappear and, finally, the magnetically disordered metallic phase becomes the only ground state. The possible models of the insulator-metal transition in $LaMnO_3$ are analyzed.

DOI: 10.1103/PhysRevB.107.144426

I. INTRODUCTION

Perovskite-like manganites $R_{1-x}A_xMnO_3$ (R = rare earth, A-alkali earth elements) exhibit a rich variety of fascinating physical phenomena extensively studied during the past few decades, including the colossal magnetoresistance, multiferroic effects, insulator-metal transition, charge and orbital ordering, and mesoscopic phase separation [1–4]. The complexity of the physical properties of these compounds is related to the strong interplay of the spin, charge, lattice, and orbital degrees of freedom. While the interplay of charge, spin, and orbital degrees of freedom can be generally analyzed in terms of the double-exchange mechanism [2,5] and Goodenough-Kanamori rules [6,7], the role of orbital-lattice coupling manifested by Jahn-Teller (JT) structural distortions and effects of electron-electron interactions remain controversial with regard to understanding the mechanisms of the colossal magnetoresistance effect and insulator-metal (IM) transition [8–14].

The parent $LaMnO_3$ compound of the orthoperovskite *Pnma* structure is the most convenient model system, allowing researchers to study effects of orbital-lattice, spin-orbital, and electron-electron coupling in the physics of manganites. The two-fold degeneracy of the half-filled e_g electronic level of high-spin Mn^{3+} ions ($t_{2g}^{\uparrow\uparrow\uparrow}e_g^{\uparrow}$) is lifted via static, cooperative JT lattice distortions, leading to the appearance of an antiferrodistortive, $d(3x^2–r^2)/d(3z^2–r^2)$, long-range orbital order below $T_{JT} \sim 750$ K and an A-type antiferromagnetic (AFM) order below $T_N = 140$ K [6,15].

In the high-pressure study of $LaMnO_3$ by Loa *et al.* [16], a continuous reduction of the cooperative JT distortion and a hidden phase transition, developing over the pressure range 7 to 18 GPa, were detected. It was assumed that the JT distortions and associated e_g orbital order fully vanish at $P \sim 18$ GPa, followed by the bandwidth-driven IM transition above 32 GPa. Later experiments showed the persistence of JT distortions in the whole pressure range up to IM transition, implying that its nature is not of conventional Mott-Hubbard type [17,18]. Subsequently, a percolative model of the pressure-induced IM transition, evolving via phase separation of the JT-distorted and -undistorted phases, and leading to occurrence of the colossal magnetoresistance effect in $LaMnO_3$, was elaborated [14,19].

Due to a strong correlation of the spin, charge, and electronic degrees of freedom, suppression of the JT distortions and e_g orbital order may affect significantly the long-range magnetic order in $LaMnO_3$ at high pressure. In the neutron diffraction study [20], a trend toward decrease of magnetic line intensities associated with the A-type antiferromagnetic order was evidenced in the pressure range 6.7 to 13 GPa. A loss of magnetic signal in ac susceptibility in $LaMnO_3$ at around 11 GPa was also reported in Ref. [21]. The hybrid density functional theory (DFT) calculations simulated compression effects on the $LaMnO_3$ ground state and predicted a formation of the ferromagnetic (FM) state in $LaMnO_3$ in the vicinity of the pressure-induced IM transition, followed at higher pressures by a magnetic moment collapse that was identified with the high-spin ($t_{2g}^{\uparrow\uparrow\uparrow}e_g^{\uparrow}$) to low-spin ($t_{2g}^{\uparrow\uparrow\uparrow\downarrow}e_g^{0}$) crossover of Mn^{3+} ions [13].

In order to explore in more detail the evolution of long-range magnetic order and its relationship with structural

*denk@nf.jinr.ru

changes in the vicinity of the IM transition, we have studied $LaMnO_3$ by means of neutron diffraction in the extended pressure range up to 39 GPa and the temperature range 5 to 290 K. For additional characterization of the local JT distortions and their evolution across the IM transition, the Raman spectroscopy experiments were performed at $T = 50$ K (below the magnetic ordering temperature) in the extended pressure range up to 50 GPa.

II. EXPERIMENTAL DETAILS

The powdered $LaMnO_3$ sample was synthesized by a standard solid-state reaction method. The mixture of La_2O_3 and $MnCO_3$ was calcinated at 900° C, then homogenized, pressed into pellets, and sintered at 1300° C for 60 h in air with several intermediate grindings. Finally, the sample was annealed at 1100° C in a vacuum. A characterization by x-ray diffraction revealed a single phase composition with lattice parameters $a = 5.7232(3)$, $b = 7.6974(5)$, and $c = 5.5334(3)$ Å, confirming nearly ideal oxygen stoichiometry, according to Ref. [22]. The neutron diffraction experiments were performed in the pressure range up to 39 GPa and the temperature range of 5 to 290 K using a DN-6 diffractometer [23] (IBR-2 pulsed reactor; JINR, Dubna, Russia). The experiments in the pressure range up to 10 GPa were performed using the sapphire anvil high-pressure cells and a sample volume of about 2 mm^3 [24]. The diffraction patterns were collected at a scattering angle of 90°, with resolution $\Delta d/d = 0.02$. The experiments in the extended pressure range up to 39 GPa were performed using a diamond anvil cell (DAC) of Boehler-Almax Plate type. The diamonds with culets of 0.8 mm and a CuBe gasket with a hole of 0.4 mm were used. The pressure inside the sapphire and diamond anvil cells was measured using the ruby fluorescence technique. The pressure gradient was less than 10% with respect to the average pressure value. The experimental data were analyzed by the Rietveld method using the Fullprof program [25].

The Raman spectra at high pressures up to 50 GPa were collected using a LabRAM HR Evolution spectrometer (Horiba, France) with a wavelength excitation of 632.8 nm emitted from a He-Ne laser, 1800 grating, a confocal hole of 200 μm, and a 20× objective. A DAC of the Boehler-Almax Plate type, diamonds with culets of 0.3 mm, and a rhenium gasket with a hole of 0.15 mm were used. The low-temperature Raman measurements were carried out using a low-vibration helium refrigerator (Advanced Research Systems, USA) at $T = 50$ K. The pressure behavior of the integrated intensities of selected Raman lines was analyzed.

III. RESULTS

A. Raman spectroscopy

In the Raman spectra measured at ambient pressure and $T = 50$ K, three well-defined lines are observed (Fig. 1). According to previous studies, they can be assigned to the B_{2g} symmetric stretching (607 cm^{-1}) and A_g antisymmetric stretching (493 cm^{-1}) vibrational modes involving in-plane oxygen ions, associated with the JT lattice distortions in the *Pnma* phase, and the A_g mode (293 cm^{-1}), associated with the out-of-phase oxygen rotations in the MnO_6 octahedra [26].

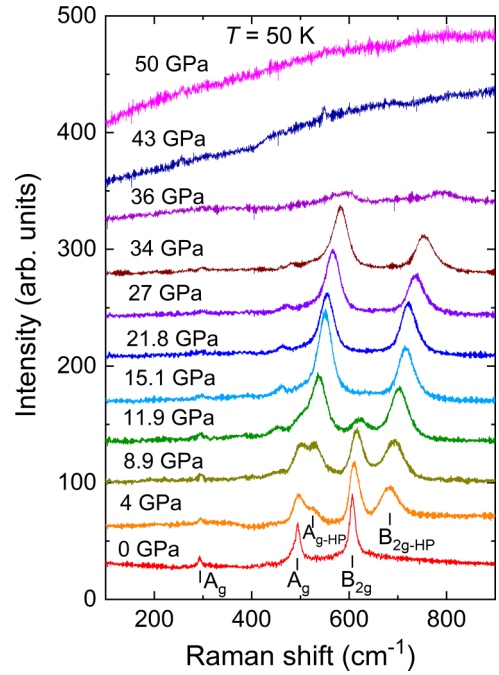

FIG. 1. Raman spectra of $LaMnO_3$ measured at selected pressures and $T = 50$ K.

At $P = 4$ GPa, an appearance of two new intense lines at 682 and 525 cm^{-1} is evidenced. Upon further compression, the integrated intensity of these lines grows [Fig. 2(a)], followed by rapid suppression of the initial B_{2g} and A_g lines. Another weaker line becomes observable at ~450 cm^{-1}. It corresponds to a bending mode of MnO_6 octahedra of A_g character, which was initially merged with the intense A_g stretching mode. At pressures above 15.1 GPa, the B_{2g} line fully vanishes, while the residual intensity of the A_g line is detected at higher pressures and it persists up to about 32 GPa (Fig. 2), where the insulator-metal transition develops. The relative intensities of the A_g and B_{2g} modes are known to be sensitive to the orientation of crystallites with respect to the laser beam direction in Raman spectroscopy measurements [27], and they can be modified strongly during a phase transformation.

These observations are associated with a gradual transition toward the perovskite phase with more regular MnO_6 octahedra due to suppressed cooperative JT distortions and long-range e_g orbital order [16,17]. The newly appeared Raman lines could be thus assigned to symmetric (B_{2g-HP}) and antisymmetric (A_{g-HP}) stretching modes of the high-pressure phase [17,28]. The fractions of coexisting structural phases [Fig. 2(b)] may be evaluated for near-surface regions of the sample in the Raman spectroscopy experiments from the integrated intensity of the relevant stretching mode peaks as f_s (f_{s-hp}) $= I_{Ag}(I_{Ag-HP})/(I_{Ag} + I_{Ag-HP})$ or equivalently, as $I_{B2g}(I_{B2g-HP})/(I_{B2g} + I_{B2g-HP})$.

Concerning the character of the pressure-induced phase, it is worth mentioning that in the ambient pressure rhombohedral and pseudocubic phases of $LaMnO_3$ that are formed successively above the Jahn-Teller transition temperature $T_{JT} = 750$ K, a persistence of local clusters involving about

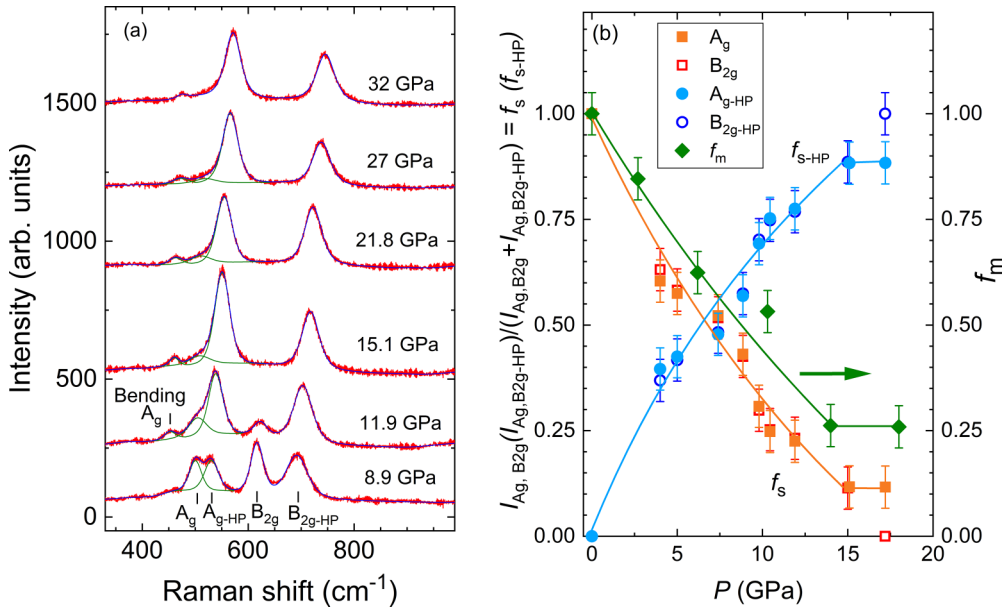

FIG. 2. Evolution of the Raman spectra of $LaMnO_3$ at $T = 50$ K over the pressure region of phase coexistence. (a) The fitting curves of individual peaks and resulting fitting curves are shown. High-pressure evolution of integrated intensities of the antisymmetric and symmetric stretching mode peaks related to the ambient-pressure (A_g, B_{2g}) and high-pressure ($A_{g-\mathrm{hp}}$, $B_{2g-\mathrm{hp}}$) phases, normalized by their summary values. (b) The pressure dependence of the volume fraction of the A-type AFM phase (f_m) at 5 K is also given for comparison.

four MnO_6 octahedra with a short-range orbital order and strong local antiferrodistortive nearest-neighbor JT coupling have been detected [29]. Somewhat similar local JT-distorted regions, but likely with a larger correlation length compared to high-temperature phases of $LaMnO_3$, are expected to occur in the pressure-induced phase of $LaMnO_3$. They giving rise to broad Raman lines, shifted to higher frequencies with respect to those in the initial orbitally ordered phase due to the more regular character of the MnO_6 octahedra. The frequency difference between the stretching modes relevant to initial and pressure-induced phases in $LaMnO_3$ at $P = 4$ GPa is ~70 and 30 cm^{-1}. These values are comparable with a shift of ~50 cm^{-1} for both modes, caused by the phase transformation from the orbitally ordered into the orbitally disordered perovskite orthorhombic phase on gallium substitution in $La_{1-x}Ga_xMnO_3$ at ambient conditions [28].

While previous Raman studies of $LaMnO_3$ were reported for a restricted pressure range up to 34 GPa [16,17], the present measurements cover a more extended pressure range up to 50 GPa, which provides better insight into the evolution of the insulator-metal transition ($P_{\mathrm{I-M}} \approx 32$ GPa). It appears that with a pressure increase from 15.1 to 32 GPa, no significant changes in Raman spectra are detected (Figs. 1 and 2), except for gradual vanishing of the residual intensity of the initial A_g line. This points to a persistence of suppressed minority regions of the JT-distorted phase up to the insulator-metal transition, in accordance with previous studies [17,18]. On further compression, the integrated intensities of the dominant Raman lines, coming from the majority pressure-induced phase, are suppressed progressively, until they vanish completely at 43 GPa. Such a behavior implies that the local JT distortions of short range or dynamic character, associated with the pressure-induced phase, finally melt upon completion of the insulator-metal transition, resulting in the disappearance of the relevant Raman lines.

B. Neutron diffraction

The neutron diffraction patterns of $LaMnO_3$, measured at selected pressures and temperatures in the sapphire (up to 10.3 GPa) and diamond (up to 39 GPa) anvil pressure cells, are shown in Fig. 3. They are consistent with the orthorhombically distorted perovskite-like structure of *Pnma* symmetry. The gradual phase transformation, revealed in the Raman experiments at pressures above 4 GPa, tunes the cooperative deformation of MnO_6 octahedra, while the average symmetry of the crystal structure likely remains unaffected. Consequently, it could not be clearly evidenced in the neutron diffraction data with a restricted resolution due to complex high-pressure experimental conditions. Therefore, we used a single-phase approach for the data treatment, in which structural parameters were considered as an average for the coexisting initial- and high-pressure phases, with the long range and local JT distortions over the gradual phase transition region.

The main focus of the present study is the characterization of cooperative JT distortions of the MnO_6 octahedra and the magnetic structure determination with regard to the pressure evolution of ordering temperature and values of Mn^{3+} magnetic moments. At ambient pressures below the Néel temperature $T_N = 140$ K, the appearance of a significant magnetic contribution to the peak (111) located at 3.51 Å and onset of the magnetic peak (012) at $d = 2.59$ Å have been evidenced, corresponding to the formation of the A-type antiferromagnetic order. The manganese-ordered magnetic moments are oriented along the *a*-axis and their value at

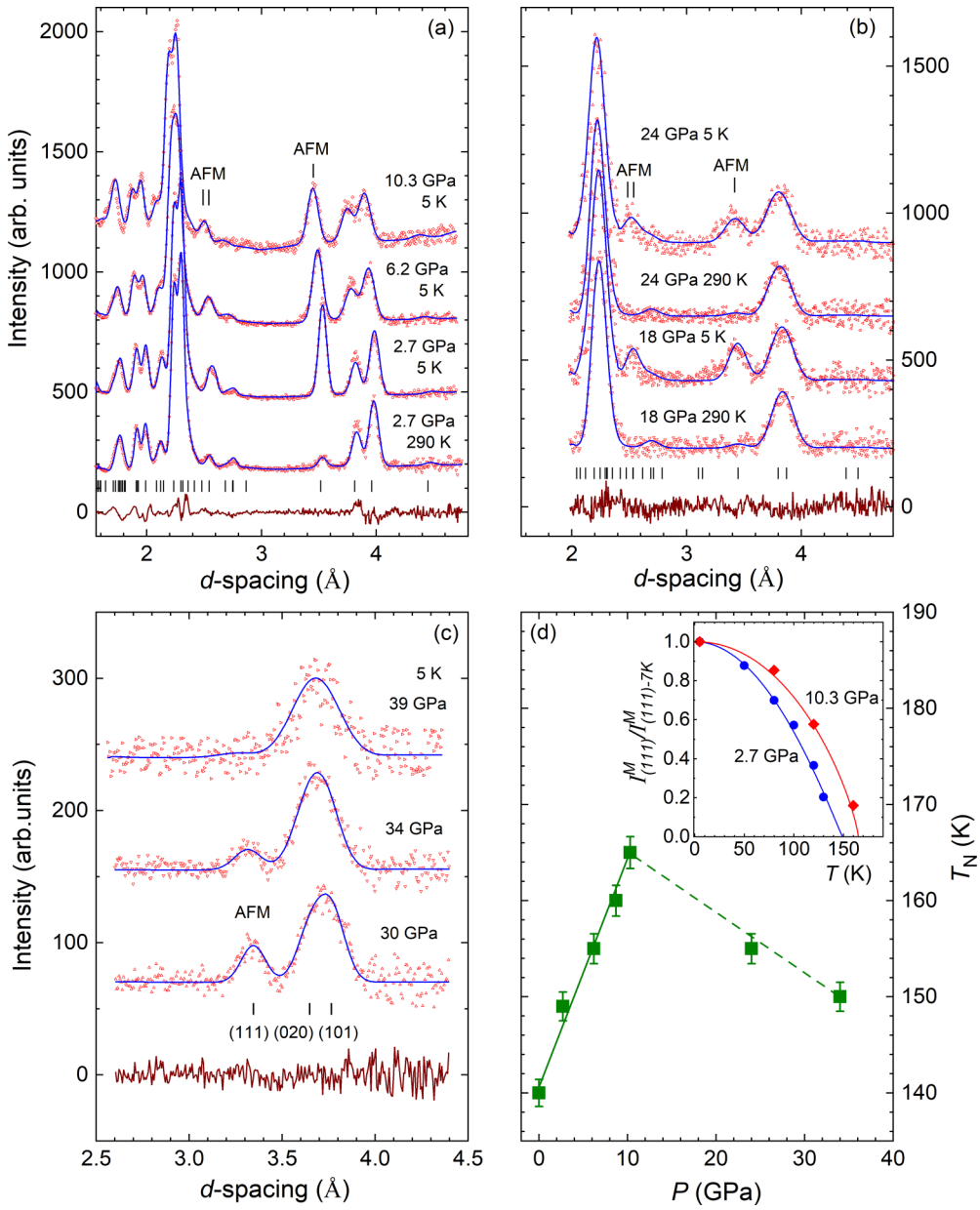

FIG. 3. Neutron diffraction patterns of $LaMnO_3$, measured at selected pressures up to 24 GPa at $T = 5$ and 290 K using sapphire (a) and diamond (b) anvil cells, and sections of the neutron diffraction patterns measured at pressures of 30 to 39 GPa and $T = 5$ K (c), processed by the Rietveld method. The experimental points, calculated profiles, and difference curves (for selected pressures 2.7 GPa at 290 K, 18 GPa at 290 K, and 30 GPa at 5 K) are shown. The ticks below represent the calculated positions of the structural peaks for $P = 2.7$ GPa (a), 18 GPa (b) at 290 K, and 30 GPa (c) at $T = 5$ K. The positions of the characteristic magnetic peaks of the A-type AFM phase are marked as "AFM". The pressure dependence of the Néel temperature of the A-type AFM phase of $LaMnO_3$ and selected temperature dependences of the magnetic contribution to integrated intensity of the (111) peak at $P = 2.7$ and 10.3 GPa (d), normalized by corresponding values at $T = 7$ K and fitted by functions $I^M_{(111)}/I^M_{(111)-7K} = [1-(T/T_N)^\alpha]^{2\beta}$ (inset).

5 K, $m_0 = 3.75(7)\,\mu_B$, is comparable with those of $\sim 3.9\,\mu_B$, found in Refs. [20,30]. The Néel temperature, evaluated from temperature dependences of the magnetic contribution to the integrated intensity of the (111) peak, obtained by subtraction of experimental data measured in the paramagnetic state, increases nearly linearly in the pressure range up to 10.3 GPa, accessible with the sapphire anvil pressure cells. The pressure coefficient $dT_N/dP = 2.5$ K/GPa [Fig. 3(d)] is comparable with one ~ 3 K/GPa, calculated from neutron diffraction data for a more restricted range up to 6.7 GPa [20]. These values are noticeably smaller in comparison with the value of ~ 5 K/GPa, estimated from magnetic susceptibility and resistivity measurements up to 2 GPa [31] and 11 GPa [21].

In the single-phase approach we used, the ordered magnetic moment and volume fraction of the magnetic phase could not be refined simultaneously from present neutron diffraction data. It is known from experimental and theoretical studies, that the manganese ordered magnetic moment in

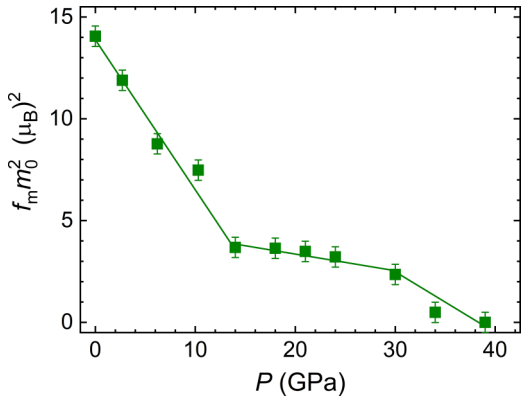

FIG. 4. The pressure dependence of the magnetic phase volume fraction multiplied by the squared ordered magnetic moment at ambient pressure at $T = 5$ K in $LaMnO_3$.

manganites is quite stable and weakly modified in the considered pressure range [13,32]. Therefore, we calculated the volume fraction (f_m) of the A-type AFM phase as a function of pressure at $T = 5$ K, keeping the ordered magnetic moment fixed to an ambient pressure value. It should be noted that the square of the effective manganese ordered moment could be evaluated as $m^2 = f_m m_0^2$. The $f_m m_0^2$ value is reduced rapidly with a pressure increase up to 10.3 GPa (Fig. 4).

The relevant, effective manganese ordered magnetic moment at $T = 5$ K is reduced from 3.75(7) to 2.7(1) μ_B. This effect may explain the loss of magnetic signal in the ac susceptibility data of $LaMnO_3$ around 11 GPa in Ref. [21].

In the orthorhombic structure of $LaMnO_3$, the MnO_6 octahedral units consist of medium-length Mn-O1 (m) bonds oriented along the b-axis, and long- and short-length Mn-O2 (l, s) bonds lying within the (ac) planes. The pressure dependences of the Mn-O bonds obtained at $T = 5$ K in the pressure range up to 10.3 GPa are shown in Fig. 5. The obtained linear compressibility coefficients [$k_{\mathrm{Mn-Oi}} = -(1/l_{\mathrm{Mn-Oi}})(dl_{\mathrm{Mn-Oi}}/dP)_T$], $k_{\mathrm{Mn-O1}} = 0.0032$, $k_{\mathrm{Mn-O2}l} = 0.0043$, and $k_{\mathrm{Mn-O2}s} = 0.0019\ \mathrm{GPa}^{-1}$ are comparable with those evaluated for the more restricted pressure range up to 6.6 GPa at ambient temperature [20]. Despite the large difference between coefficients for the Mn-O2 (l) and (s) bonds, their average value $k_{\mathrm{Mn-O2}} = 0.0031\ \mathrm{GPa}^{-1}$ is about the same as for the Mn-O1 (m) bond. The degree of the static cooperative distortion of the MnO_6 octahedra may be characterized by a coefficient

$$\delta_{\mathrm{JT}} = \left(\frac{1}{3} \sum_i (l_{\mathrm{Mn-Oi}} - \langle l_{\mathrm{Mn-O}} \rangle)^2 \right)^{1/2}, \qquad (1)$$

where summation is taken over three types of Mn-O bonds and $\langle l_{\mathrm{Mn-O}} \rangle$ is the average Mn-O bond length. The δ_{JT} coefficient is reduced by 20%, from 0.120 to 0.096 Å, in the 0 to 10.3 GPa pressure range [Fig. 5(c)]. This reduction rate is comparable with one evaluated from the XAS data [18]. The Mn-O1-Mn bond angle increases nearly linearly from 155.1(3) to 158.5(3)° with a pressure increase up to 10.3 GPa at $T = 5$ K. The Mn-O2-Mn bond angle grows from 157.3(3) to 158.8(3)° at pressures up to 6.2 GPa and it varies weakly at higher pressures up to 10.3 GPa. This peculiar pressure behavior may be associated with a suppression of the cooperative JT distortions within the (ac) planes and phase coexistence, which is not clearly detectable in the neutron diffraction data.

Alternatively, the local JT distortions of MnO_6 octahedra are expressed through E_g symmetry deformation modes of the regular octahedron $Q_2 = 2(l-s)/\sqrt{2}$ and $Q_3 = 2(2m-l-s)/\sqrt{6}$ [33]. Their values, presented in Fig. 5(d), show that the Q_2 component is 0.400 at ambient pressure and exhibits a pronounced reduction at high pressure up to 10.3 GPa by about 20%, while the Q_3 component is −0.107 at ambient pressure with a much weaker pressure-induced absolute value reduction of about 5%. The bonding orbitals, describing the e_g electron state, can be expressed as $\Psi_g = \cos(\varphi/2)d(3z^2-r^2) + \sin(\varphi/2)d(x^2-y^2)$, where angle φ, characterizing the orbital mixing coefficients, is determined as $\tan\varphi = Q_3/Q_2$ [33,34]. The relevant values of $\varphi = -15.0$ and $-17.9°$, obtained at ambient pressure and 10.3 GPa, reflect a decreasing tendency of the $d(3z^2-r^2)$ orbitals population via reduction of the $\cos(\varphi/2)$ coefficient. Although, the calculated change in this pressure range is quite small: about 0.5%.

We now turn to neutron diffraction results in the pressure range up to 39 GPa [Fig. 3(c)]. Due to a more limited d spacing range in experiments with diamond anvil cells, it was difficult to evaluate accurately the full set of structural parameters necessary for an analysis of the bond distance behavior at pressures above 10.3 GPa. As indirect evidence of a gradual transition to the pressure-induced phase with suppressed cooperative JT distortions, merging of initially split peaks (101)/(020) at ∼3.9 Å and (022)/(220) at ∼2.25 Å at higher pressures was found (Fig. 3). Consequently, the investigation was restricted to evolution of the magnetic structure. The results presented in Fig. 4 show that the $f_m m_0^2$ value continues its rapidly decreasing trend upon compression up to 14 GPa, and the effective ordered magnetic moment value is reduced to 1.9(1) μ_B. In the pressure range 14 to 30 GPa it becomes a weakly pressure variable. Above 30 GPa, a rapid collapse of the $f_m m_0^2$ value occurs, with full vanishing of the AFM phase at 39 GPa. Simultaneously, the temperature-dependent experiments evidence a drop of Néel temperature from 165 K at 10.3 GPa to about 150 K at 34 GPa [Fig. 3(d)].

IV. DISCUSSION

The observed magnetic behavior of $LaMnO_3$ at high pressure can be explained in the following scenario. The stability of the A-type AFM state is intimately related to the presence of e_g orbital order and associated JT structural distortions, the character of which modifies from a long range to local one in the ambient- and high-pressure structural phases. In this magnetic state, the dominant in-plane superexchange interaction J_{ab} between half-filled and empty e_g orbitals of Mn^{3+} neighbors is responsible for formation of the ferromagnetic (ac) planes, which are coupled antiferromagnetically along the b-axis by the superexchange interaction J_c via the t_{2g} orbitals. In the mean field approximation [34],

$$T_N \sim E_{\mathrm{A-typeAFM}} \sim (-4J_{ab} + 2J_c). \qquad (2)$$

According to the inelastic neutron scattering study [30], the value of $J_{ab} = -0.83$ meV is about 1.5 times larger in

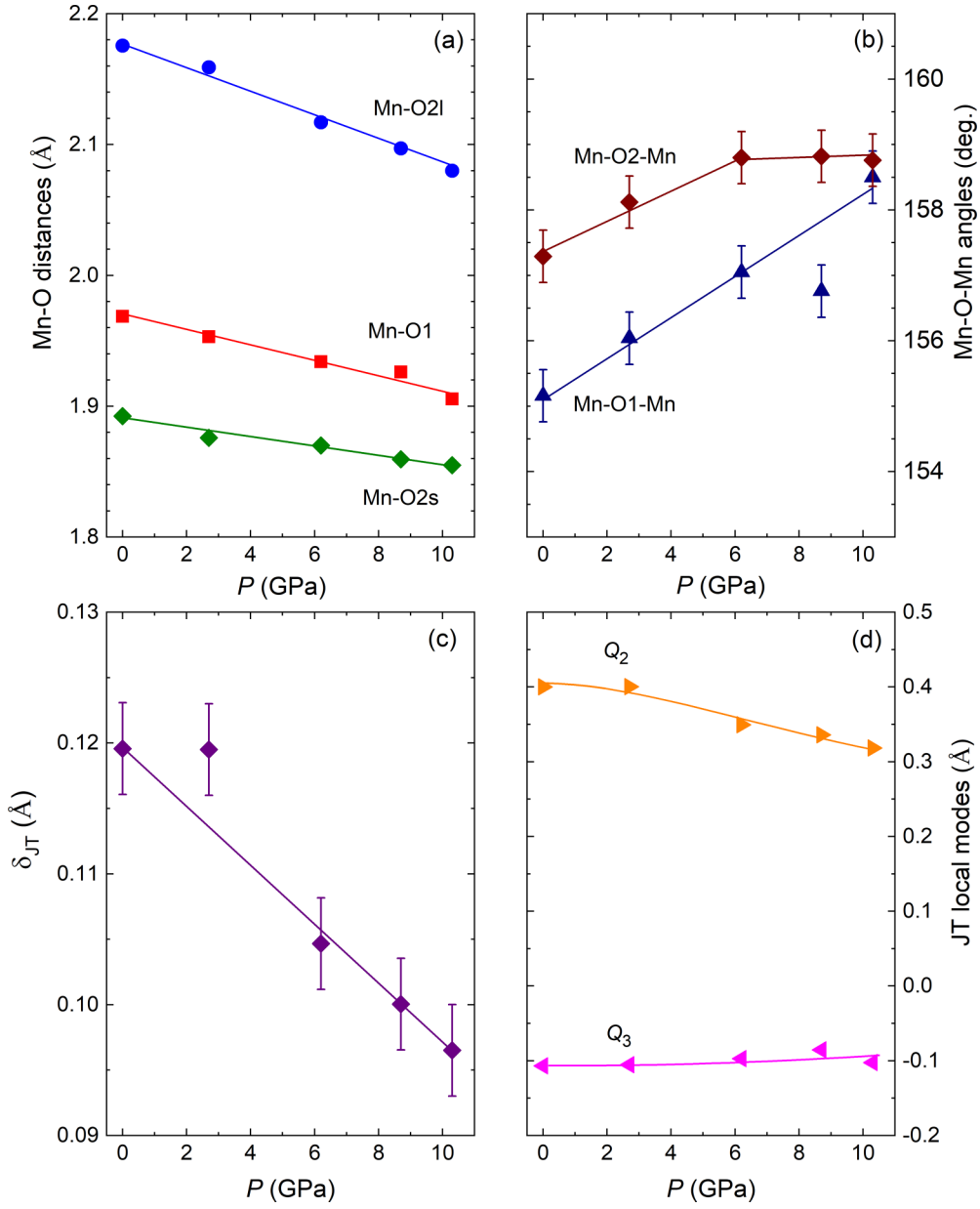

FIG. 5. The pressure dependence of Mn-O distances (error bars are within the symbol sizes) (a), average Mn-O-Mn bond angle (b), JT distortion parameter (c), and JT local modes Q_2 and Q_3 (d) in $LaMnO_3$ at $T = 5$ K.

comparison with $J_c = 0.58$ meV. The Mn-O distance dependence of the effective J_{ab} and J_c parameters can be evaluated as $J_{ab} \sim \langle l_{\mathrm{Mn-O2}} \rangle^{-7}$ and $J_c \sim (l_{\mathrm{Mn-O1}})^{-7}$. It takes into account scaling of the effective electron transfer integrals $t_{ab,c} \sim (l_{\mathrm{Mn-O2,1}})^{-7/2}$, which was determined by a combination of the electron transfer processes contributing to in-plane and interplane superexchange interactions and involving e_g, t_{2g} orbitals of Mn^{3+} ions and p orbitals of O^{2-} ions, and relationships $J_{ab} \sim t_{ab}^2$, $J_c \sim t_c^2$ [12,35]. From the experimentally determined pressure dependences of Mn-O1,2 distances and Eq. (2), one can calculate the Néel temperature to increase with the pressure coefficient $dT_N/dP = 3.5$ K/GPa. This agrees well with the previously mentioned values $dT_N/dP =$ 2.5 to 3.0 K/GPa obtained from the neutron diffraction data in the present study and Ref. [20]. For clarity, a weak pressure variation of the Mn-O-Mn bond angles was neglected in this consideration.

According to previous studies [16–20], supported by present results, the static cooperative distortions are suppressed gradually in the ambient-pressure phase, and the new structural phase containing more regular MnO_6 octahedra with only dynamic or short-range JT distortions is formed gradually at high pressures. In order to get a more detailed insight into the structural origin of the residual A-type AFM regions observed at high pressures, one may compare the pressure behavior of the initial and pressure-induced structural phase fractions $f_s(f_{s-\mathrm{hp}})$ evaluated by the Raman spectroscopy measurements with the fraction of the AFM phase f_m, obtained by neutron diffraction. Generally, both the f_m and f_s values demonstrate a remarkably close relationship

in the phase coexistence region [Fig. 2(b)]. This provides reasonable evidence that the vanishing A-type AFM order is associated with the gradually suppressed structural phase possessing static cooperative JT distortions. Such a model is also consistent with the observation of residual Raman lines related to the initial phase with static cooperative JT distortions, persistent up to the insulator-metal transition, in previous Raman studies [17]. At pressures above 10 GPa, some difference between the f_m and f_s fractions is found. It could be related to the fact that the neutron diffraction is sensitive to volume-averaged characteristics, while Raman spectroscopy is sensitive to surface-averaged characteristics of the system.

In the pressure range of phase coexistence, the relative volume fraction of the A-type AFM regions, associated with a suppressed initial phase with static cooperative JT distortions, is evaluated as 53% at 10.3 GPa and 26% at 14 GPa [Fig. 2(b)], neglecting hybridization effects. At higher pressures, persistence of the suppressed minority regions of the initial JT-distorted phase is evidenced in the Raman measurements (Fig. 2). The evaluated volume fraction of residual regions of the A-type AFM phase is reduced to about 17% at 30 GPa. The relevant magnetic correlation length may be evaluated from neutron diffraction data using the Selyakov-Scherrer formula as $\xi = 2\pi/\Delta q_{(111)} = d^2_{(111)}/\Delta d_{(111)}$, where $\Delta q_{(111)}$, $\Delta d_{(111)}$, and $d_{(111)}$ are the full widths at half maximum in the q and d space and position of the (111) magnetic peak of the A-type AFM phase, respectively. The value $\xi \approx 140$ Å was obtained for $P = 30$ GPa at 5 K. This provides a scale of about 35 MnO_6 octahedral units and gives additional support that the residual A-type AFM regions are associated with persistent minority regions of the initial structural phase with the static cooperative JT distortions. For local JT-distorted structural regions, a typical correlation length covering up to 5 to 10 MnO_6 units should be expected.

In the vicinity of the insulator-metal transition, found in $LaMnO_3$ at 32 to 34 GPa [16,17], a rapid suppression of the magnetic intensity of the (111) diffraction peak at 5 K occurs, and its complete disappearance is evidenced at 39 GPa [Fig. 3(c)]. This observation points to a total suppression of the residual regions of the A-type AFM state, correlating with the vanishing of the Raman lines associated with the local JT-distorted regions in the pressure-induced phase (Figs. 1 and 2). The suppression of the e_g orbital order is expected to result in the enhancement of the FM superexchange interactions between nearly degenerate e_g orbitals, and DFT calculations indeed predict the stabilization of the FM phase at pressures above 11 GPa in $LaMnO_3$ [13]. Nevertheless, the neutron diffraction data at 39 GPa [Fig. 3(c)] did not show any signatures of additional magnetic intensity that could be related to FM or AFM long-range magnetic ordering. Therefore, the magnetic ground state of the pressure-induced metallic phase is likely of a paramagnetic or short-range ordered spin glass character.

The nature of the pressure-induced insulator-metal transition in $LaMnO_3$ has been extensively debated but still remains unclear. There are numerous theoretical scenarios that consider competing electron-electron and electron-lattice interactions. They include a transition from the JT-distorted orbitally polarized insulating phase into an undistorted orbitally unpolarized metallic phase [12], overlapping of e_g subbands in the phase with a finite JT distortion [11], and progressive suppression of the JT distortions with a correlated change of the magnetic order from AFM to FM at lower pressures, followed by closing of the energy gap between e_g subbands after the transition to an undistorted phase has been completed at higher pressures [13]. In contrast, there is a percolative model [17] that anticipates that regions of the pressure-induced phase, found to appear gradually in $LaMnO_3$ by Raman spectroscopy, are metallic. The insulator-metal transition starts in the mixed inhomogeneous phase state, also containing regions of the initial, distorted insulating phase, when the undistorted metallic phase volume fraction exceeds a percolative threshold of 0.29.

In this regard, the present neutron diffraction data bring important details that demonstrate large complexity of the pressure-induced behavior of $LaMnO_3$. The reduction of the effective ordered magnetic moment of about two times in the pressure range 0 to 14 GPa at $T = 5$ K is associated with a progressive suppression of the JT-distorted structural phase with an A-type AFM ordered magnetic ground state and stabilization of the magnetically disordered phase with more regular MnO_6 octahedra, which coexist in the form of nanoscale regions. Since the evaluated volume fraction of the pressure-induced phase regions, based on both neutron diffraction ($1-f_m$) and Raman ($f_{s-\mathrm{hp}}$) measurements exceeds 50% in this pressure range (Fig. 2), which should lead to onset of the metallic phase in the percolative model of the insulator-metal transition [17] at $P < 14$ GPa, i.e., much below the actually found transition at 32 GPa. A slower reduction of the volume fraction of the AFM phase in the pressure range of 14 to 30 GPa (Fig. 4) indicates comparable energies of the coexisting phases. This points to a case of continuous transition, where static JT distortions are gradually transformed to dynamic ones. Another open question concerns the rapid vanishing of the ordered magnetic moment above 30 GPa (Fig. 4). In the absence of formation of long-range magnetically ordered states, this may be a signature of closing the gap between e_g subbands, which results in a conduction channel of the $e_g\uparrow$ character. The DFT calculations predict that at the further relative volume reduction of just 2.5% with respect to one corresponding to the insulator-metal transition pressure, the high-spin to low-spin crossover develops progressively in $LaMnO_3$ [13]. This provides an additional mechanism for a pressure-induced population of the $t_{2g}\downarrow$ carriers and their final dominance in electric conduction. As a result, realization of the pressure-induced transport half-metal state in $LaMnO_3$ is predicted [13], which is similar to those found in optimally doped manganites with a colossal magnetoresistance effect like $La_{0.7}Sr_{0.3}MnO_3$.

V. CONCLUSIONS

The neutron diffraction and Raman spectroscopy study of $LaMnO_3$ at ambient and high pressures provides important details on the evolution of long-range magnetic order during the gradual phase transformation at high pressures. It is evidenced that melting of the static cooperative JT distortions and e_g orbital order, accompanied by a reduction of the absolute values of the Q_2 and Q_3 local JT modes, leads to gradual suppression

of the A-type AFM order and a rapid reduction of the effective ordered manganese magnetic moment. The residual regions of the suppressed A-type AFM phase, associated with the JT distortions, coexist with the magnetically disordered phase up to 30 GPa. At further compression, these regions finally vanish in a rather steep manner, and the magnetically disordered metallic phase becomes the ground state. The metallicity of the high-pressure $LaMnO_3$ phase is further enhanced by modification of electronic bands at the vicinity of the Fermi level and consequent spin-state crossover at manganese sites.

The electron-lattice and electron-electron interactions play a decisive role in development of the insulator-metal transition in $LaMnO_3$ via progressive suppression of the e_g orbital order, mediated long-range cooperative JT distortions, and reduction of the bandgap, while the role of percolative mechanisms is less important.

ACKNOWLEDGMENT

We acknowledge O. N. Lis for assistance with Raman measurements.

[1] *Colossal Magnetoresistance Oxides*, edited by Y. Tokura (Gordon and Breach, New York, 2000).
[2] E. Dagotto, T. Hotta, and A. Moreo, Phys. Rep. **344**, 1 (2001).
[3] T. Kimura, T. Goto, H. Shintani, K. Ishizaka, T. Arima, and Y. Tokura, Nature (London) **426**, 55 (2003).
[4] T. Kimura, Annu. Rev. Mater. Res. **37**, 387 (2007).
[5] P.-G. de Gennes, Phys. Rev. **118**, 141 (1960).
[6] J. B. Goodenough, *Magnetism and the Chemical Bond* (Interscience, New York, 1963).
[7] J. Kanamori, J. Phys. Chem. Solids **10**, 87 (1959).
[8] A. J. Millis, P. B. Littlewood, and B. I. Shraiman, Phys. Rev. Lett. **74**, 5144 (1995).
[9] W.-G. Yin, D. Volja, and W. Ku, Phys. Rev. Lett. **96**, 116405 (2006).
[10] G. Trimarchi and N. Binggeli, Phys. Rev. B **71**, 035101 (2005).
[11] A. Yamasaki, M. Feldbacher, Y.-F. Yang, O. K. Andersen, and K. Held, Phys. Rev. Lett. **96**, 166401 (2006).
[12] J. D. Fuhr, M. Avignon, and B. Alascio, Phys. Rev. Lett. **100**, 216402 (2008).
[13] J. He, M.-X. Chen, X.-Q. Chen, and C. Franchini, Phys. Rev. B **85**, 195135 (2012).
[14] M. Baldini, T. Muramatsu, M. Sherafati, H.-K. Mao, L. Malavasi, P. Postorino, S. Satpathy, and V. V. Struzhkin, Proc. Natl. Acad. Sci. USA **112**, 10869 (2015).
[15] J. Rodríguez-Carvajal, M. Hennion, F. Moussa, A. H. Moudden, L. Pinsard, and A. Revcolevschi, Phys. Rev. B **57**, R3189 (1998).
[16] I. Loa, P. Adler, A. Grzechnik, K. Syassen, U. Schwarz, M. Hanfland, G. K. Rozenberg, P. Gorodetsky, and M. P. Pasternak, Phys. Rev. Lett. **87**, 125501 (2001).
[17] M. Baldini, V. V. Struzhkin, A. F. Goncharov, P. Postorino, and W. L. Mao, Phys. Rev. Lett. **106**, 066402 (2011).
[18] A. Y. Ramos, N. M. Souza-Neto, H. C. N. Tolentino, O. Bunau, Y. Joly, S. Grenier, J.-P. Itié, A.-M. Flank, P. Lagarde, and A. Caneiro, Europhys. Lett. **96**, 36002 (2011).
[19] M. Sherafati, M. Baldini, L. Malavasi, and S. Satpathy, Phys. Rev. B **93**, 024107 (2016).
[20] L. Pinsard-Gaudart, J. Rodríguez-Carvajal, A. Daoud-Aladine, I. Goncharenko, M. Medarde, R. I. Smith, and A. Revcolevschi, Phys. Rev. B **64**, 064426 (2001).
[21] J.-S. Zhou, Y. Uwatoko, K. Matsubayashi, and J. B. Goodenough, Phys. Rev. B **78**, 220402(R) (2008).
[22] J. Töpfer and J. B. Goodenough, J. Solid State Chem. **130**, 117 (1997).
[23] D. P. Kozlenko, S. E. Kichanov, E. V. Lukin, and B. N. Savenko, Crystals **8**, 331 (2018).
[24] D. P. Kozlenko, S. E. Kichanov, E. V. Lukin, and B. N. Savenko, Cryst. Rep. **66**, 303 (2021).
[25] J. Rodríguez-Carvajal, Phys. B **192**, 55 (1993).
[26] M. N. Iliev, M. V. Abrashev, J. Laverdière, S. Jandl, M. M. Gospodinov, Y.-Q. Wang, and Y.-Y. Sun, Phys. Rev. B **73**, 064302 (2006).
[27] M. N. Iliev, M. V. Abrashev, H.-G. Lee, V. N. Popov, Y. Y. Sun, C. Thomsen, R. L. Meng, and C. W. Chu, Phys. Rev. B **57**, 2872 (1998).
[28] M. Baldini, D. Di Castro, M. Cestelli-Guidi, J. Garcia, and P. Postorino, Phys. Rev. B **80**, 045123 (2009).
[29] X. Qiu, Th. Proffen, J. F. Mitchell, and S. J. L. Billinge, Phys. Rev. Lett. **94**, 177203 (2005).
[30] F. Moussa, M. Hennion, J. Rodríguez-Carvajal, H. Moudden, L. Pinsard, and A. Revcolevschi, Phys. Rev. B **54**, 15149 (1996).
[31] J.-S. Zhou and J. B. Goodenough, Phys. Rev. B **68**, 054403 (2003).
[32] D. P. Kozlenko, I. N. Goncharenko, B. N. Savenko, and V. I. Voronin, J. Phys.: Condens. Matter **16**, 6755 (2004).
[33] J. Kanamori, J. Appl. Phys. **31**, S14 (1960).
[34] H. Zenia, G. A. Gehring, and W. M. Temmerman, New J. Phys. **7**, 257 (2005).
[35] J. W. Liu, Z. Zeng, Q. Q. Zheng, and H. Q. Lin, Phys. Rev. B **60**, 12968 (1999).